AIAA JOURNAL
Vol. 34, No. 8, August 1996

Explicit Unconditionally Stable Approaches for Built-Up Shell Structural Configurations

Xiaoqin Chen,* Kumar K. Tamma,† and Desong Sha‡
University of Minnesota, Minneapolis, Minnesota 55455

Built-up structures, especially those involving shell-type components, are encountered in many areas of engineering. Since full three-dimensional modeling may be cost prohibitive, shell-type elements have played an important role in dynamic simulations; however, the nonlinear dynamic analysis is still relatively expensive because of the enormous computations involved. Most often, implicit approaches such as the Newmark $\beta = 0.25$ are commonly employed. With the motivation of further enhancing the accuracy and efficiency of analysis of large practical structural problems, we describe explicit, unconditionally stable approaches newly developed by the authors to analyze the dynamics of linear/nonlinear shell structures and subsequently show the applicability to large-scale practical structural dynamics problems. The explicit nature of the formulations and the unconditionally stable algorithmic stability and excellent algorithmic attributes in conjunction with efficient numerical computational features indeed lend themselves well for the analysis of a wide class of complex shell-type structural configurations. The computational and implementation aspects and the numerical evaluation of the so-called VIP (virtual-pulse) time integral methodology that inherits these attributes for general shell-type structural dynamics problems are presented here. Comparisons are also drawn between the VIP methodology and the Newmark family of methods on the aspects of the accuracy and computing time. The numerical results given, which were performed on the Cray supercomputer, show the applicability of the VIP methodology for practical problems, and the computations demonstrate the significant reduction in computing time compared with the most widely advocated Newmark family of methods for given accuracy conditions.

Introduction

SHELL structures and structural configurations are encountered in a great variety of industrial applications to include aircraft structures, various tanks and pressure vessels, automobile bodies, gas turbine engine cases, and the like. As such, the dynamic behavior of general shell structures under transient loading is of widespread interest in many aerospace, automotive, mechanical, civil, and other related industries. The configurations of shell structures may have forms such as curved surfaces, stiffened panels in one or more directions, laminated composite, and the like. The analysis of these structures is based on the fundamental laws of solid continuum mechanics. With different engineering applications, there exist several types of shell analysis: stress and deflection analysis, buckling, vibration, dynamic response, fluid/structure and thermal-structure interactions, and the like.

Attention is focused in this paper on the transient response of shells influenced by varying mechanical loads employing a new methodology of computation recently developed by the authors.[1,2] For practical geometric shell-type configurations encountered in engineering practice, almost all methods of dynamic shell analysis involve the use of numerical methods. In general, these analysis methods involve analytical approaches via classical reduction of the associated differential equations to algebraic equations that are then solved numerically or numerical techniques where the differential governing equations are first replaced (discretized) by the corresponding numerical counterparts and then solved computationally via numerical algorithms. Since closed-form solutions and routine experimental investigations may not be practical and are cumbersome or cost prohibitive as the case may be for practical shell-type structural configurations, numerical methods of approach are most frequently relied upon and are a viable alternative.

Of the various numerical methods employed for the discretization of a continuum, the finite element method has become an industry standard and widely accepted in the community at large. Some distinct approaches involving finite element discretized representations for shell structures have involved flat triangular or quadrilateral elements; curved elements, formulated on the basis of various shell theories; and elements derived from three-dimensional formulations by the use of degeneration techniques[3,4] such as that introduced by Ahmad et al.[4] for linear analysis of moderately thick shells. Other related efforts for applications to linear and nonlinear shell structures are available in the literature.[5-9] In the present paper, we adopt the degenerate shell formulations for the numerical space discretization.

For transient analysis of shell structures, much of the past efforts following the semidiscretization process have been attempted employing time integration techniques such as the widely advocated Newmark family of methods,[10,11] although use of mode superposition has been of interest for determining the response of linear structural components. Because of the intensity of the computations involved in the modeling/analysis of complex structural shell configurations encountered in engineering practice, especially nonlinear transient analysis, not only the accuracy is of importance, but also the computing expense and time involved in the analysis and convergence of results, in addition to computer storage necessities, dominate large-scale computations. The totality of these considerations directly influence the feasibility for conducting an analysis, and routine analysis may be impractical in certain situations.

With the motivation to overcome some of the existing difficulties and deficiencies to further improve upon the accuracy, speed-up, and convergence of computations for general linear/nonlinear dynamic analysis of large, complex shell-type structural configurations, and to develop techniques suitable for parallel computations on modern, high-speed computing environments, recently the authors have developed the so-called virtual-pulse (VIP) time integral methodology for general structural dynamic problems.[1,2] In these papers, the authors have theoretically demonstrated that the VIP methodology possesses several improved algorithmic characteristics with

Received March 24, 1994; revision received May 3, 1995; accepted for publication Nov. 11, 1995.

*Graduate Research Assistant, Department of Mechanical Engineering, 111 Church St. SE; currently Applications Engineer Specialist, MARC Analysis Research Corporation/Midwest, 24 Frank Lloyd Wright Drive, Ann Arbor, MI 48106.

†Professor, Department of Mechanical Engineering, 111 Church St. SE.

‡Visiting Research Scholar, Department of Mechanical Engineering; currently Professor, Dalian University of Technology, Dalian, People's Republic of China.

computationally attractive numerical attributes while maintaining a high degree of accuracy. Preliminary efforts following the theoretical developments for linear/nonlinear structural dynamic models[12] have shown significant promise and potential of the VIP methodology as a viable alternative to traditional practices. A definite purpose of developing these techniques is no doubt to provide robust computational tools to handle complex structural configurations of large-scale geometric models encountered in engineering practice with features for improved efficiency and accuracy in conjunction with attractive computational and algorithmic characteristics suitable for high-speed computing environments.

In the present paper, we focus attention on the development and applicability of the VIP methodology of computation to large-scale dynamic analysis of elastoplastic/elastic shell structures and built-up shell structural configurations discretized by various types of shell elements. Subsequently we also evaluate the proposed developments by drawing relevant comparisons with the widely advocated Newmark family of methods on the aspects of accuracy and computing time. We first summarize the general theory relevant to the dynamic formulations and the resulting explicit, unconditionally stable VIP time integral methodology. Subsequently, we demonstrate the implementation of the approach and the applicability to numerous illustrative numerical test models for practical elastic/elastic-plastic shell structures including comparisons to traditional practices whenever feasible. The computational efforts were performed at the Minnesota Supercomputer Institute (MSI) on the Cray 2.

Dynamic Analysis of General Shell Structures: Explicit VIP Methodology

The dynamic force equilibrium of a typical node in a system of structural elements at any time station t can be expressed by

$$\boldsymbol{F}^i + \boldsymbol{F}^d + \boldsymbol{f}^r = \boldsymbol{P} \tag{1}$$

where

$\boldsymbol{F}^i$ = inertial force vector
$\boldsymbol{F}^d$ = damping force vector
$\boldsymbol{f}^r$ = internal resisting force vector
$\boldsymbol{P}$ = vector of externally applied forces

In this paper, merely for purposes of illustration, we only consider situations without damping effects. At time station t, let $\delta \boldsymbol{u}$ be the vector of virtual displacements, $\delta \varepsilon$ the vector of associated virtual strains, σ the vector of stresses, and ρ the mass density. From the standard finite element representation, the displacement and strains and also their virtual counterparts are approximated as

$$\boldsymbol{u} = \sum_{i=1}^{r} \boldsymbol{N}_i[\boldsymbol{d}_i] \qquad \delta \boldsymbol{u} = \sum_{i=1}^{r} \boldsymbol{N}_i[\delta \boldsymbol{d}_i] \tag{2a}$$

$$\varepsilon = \sum_{i=1}^{r} \boldsymbol{B}_i[\boldsymbol{d}_i] \qquad \delta \varepsilon = \sum_{i=1}^{r} \boldsymbol{B}_i[\delta \boldsymbol{d}_i] \tag{2b}$$

where $\boldsymbol{d}_i$ is the vector of nodal displacements, $\delta \boldsymbol{d}_i$ the vector of virtual nodal displacements, $\boldsymbol{N}_i$ the matrix of shape functions, and $\boldsymbol{B}_i$ the strain-displacement matrix. The total number of nodes for the element is r. The dynamic force equilibrium for each element then can be written in the domain of the element $\boldsymbol{V}$ by the principle of virtual work as (in the absence of damping)

$$\boldsymbol{F}^i + \boldsymbol{f}^r = \boldsymbol{P} \tag{3}$$

where

$$\boldsymbol{F}^{i(e)} = \left[\int_v \boldsymbol{N}^{(e)^T} \rho \boldsymbol{N}^{(e)} dV\right] \boldsymbol{a}^{(e)} = \left[\boldsymbol{M}^{(e)}\right]\left\{\boldsymbol{a}^{(e)}\right\} \tag{4a}$$

$$\boldsymbol{f}^{r(e)} = \int_v \boldsymbol{B}^{(e)^T} \left\{\sigma^{(e)}\right\} dV \tag{4b}$$

Merely for clarity and for purposes of illustration, the relationship between displacement and strain and between stress and strain for linear and nonlinear shell elements follows next.

Element Representations

Degenerate shell elements are employed in this study following previous efforts[3-6] and the basic assumptions adopted are that 1) normals to middle surface remain straight after deformation and 2) the stress component normal to the middle surface is constrained to be zero in the constitutive model equations.

The relevant degrees of freedom (DOF) at a typical node in the element corresponded to three translations and two rotations of the normal at the node.

Figure 1 shows the representative coordinate system employed.

The coordinates of a point in the element in the curvilinear system (ξ, η, ζ) are related to the element interpolation function $N_k(\xi, \eta)$ where $k = 1, 2, \ldots, r$ and correspond to ζ = constant surface as

$$\boldsymbol{x}_i = \sum_{k=1}^{r} \boldsymbol{N}_k(\xi, \eta) \boldsymbol{x}_{ik,\text{mid}} + \sum_{k=1}^{r} \boldsymbol{N}_k(\xi, \eta) \frac{t_k}{2} \zeta \hat{\boldsymbol{V}}_{3k}^i \tag{5}$$

where r is the number of element nodes, t_k is the thickness at node k, and $\boldsymbol{V}_{3k} = \boldsymbol{x}_k^{\text{top}} - \boldsymbol{x}_k^{\text{bot}}$ with $\hat{\boldsymbol{V}}_{3k} = \boldsymbol{V}_{3k}/|\boldsymbol{V}_{3k}|$. A typical element displacement field is approximated as

$$\boldsymbol{u} = \boldsymbol{N}\delta \tag{6}$$

where $\delta^T = [\delta_1, \delta_2, \ldots, \delta_n]^T$ are the element nodal variables. The element displacement field $\boldsymbol{u}^T = [\boldsymbol{u}, \boldsymbol{v}, \boldsymbol{w}]^T$ are given as

$$\boldsymbol{u}_i = \sum_{k=1}^{r} \boldsymbol{N}_k \boldsymbol{u}_{ik,\text{mid}} + \sum_{k=1}^{r} \boldsymbol{N}_k \frac{t_k}{2} \zeta \left(\hat{\boldsymbol{V}}_{1k}^i \beta_{1k} - \hat{\boldsymbol{V}}_{2k}^i \beta_{2k}\right) \tag{7}$$

where $\boldsymbol{V}_{1k}$ is perpendicular to $\boldsymbol{V}_{3k}$ and parallel to the global x–z plane, $\boldsymbol{V}_{2k} = \boldsymbol{V}_{3k} \times \boldsymbol{V}_{1k}$; $\hat{\boldsymbol{V}}_{1k} = \boldsymbol{V}_{1k}/|\boldsymbol{V}_{1k}|$ and $\hat{\boldsymbol{V}}_{2k} = \boldsymbol{V}_{2k}/|\boldsymbol{V}_{2k}|$, and β_{1k} and β_{2k} are the two rotations.

A local coordinate set $\boldsymbol{x}_i'$ is a Cartesian system defined at the sampling points where stress and strain measures are calculated. A typical direction $\boldsymbol{x}_3'$ is perpendicular to the surface ζ = constant. The direction $\boldsymbol{x}_1'$ is taken tangent to the ξ direction at the sampling point. For the load system $\boldsymbol{x}_i'$ where $\boldsymbol{u}'$, $\boldsymbol{v}'$, and $\boldsymbol{w}'$ are the associated displacement components, the strains are typically expressed as

$$\varepsilon^T = [\boldsymbol{u}'_{,x'}, \boldsymbol{v}'_{,y'}, \boldsymbol{u}'_{,y'} + \boldsymbol{v}'_{,x'}, \boldsymbol{u}'_{,z'} + \boldsymbol{w}'_{,x'}, \boldsymbol{v}'_{,z'} + \boldsymbol{w}'_{,y'}] \tag{8}$$

and the relation between the local and global derivatives is given as

$$\begin{bmatrix} \boldsymbol{u}'_{,x'} & \boldsymbol{v}'_{,x'} & \boldsymbol{w}'_{,x'} \\ \boldsymbol{u}'_{,y'} & \boldsymbol{v}'_{,y'} & \boldsymbol{w}'_{,y'} \\ \boldsymbol{u}'_{,z'} & \boldsymbol{v}'_{,z'} & \boldsymbol{w}'_{,z'} \end{bmatrix} = \boldsymbol{T}^T \begin{bmatrix} \boldsymbol{u}_{,x} & \boldsymbol{v}_{,x} & \boldsymbol{w}_{,x} \\ \boldsymbol{u}_{,y} & \boldsymbol{v}_{,y} & \boldsymbol{w}_{,y} \\ \boldsymbol{u}_{,z} & \boldsymbol{v}_{,z} & \boldsymbol{w}_{,z} \end{bmatrix} \boldsymbol{T} = \boldsymbol{T}^T \boldsymbol{U} \boldsymbol{T} \tag{9a}$$

where $\boldsymbol{T}$ is the transformation matrix defining the direction cosines between the local and global coordinate systems.

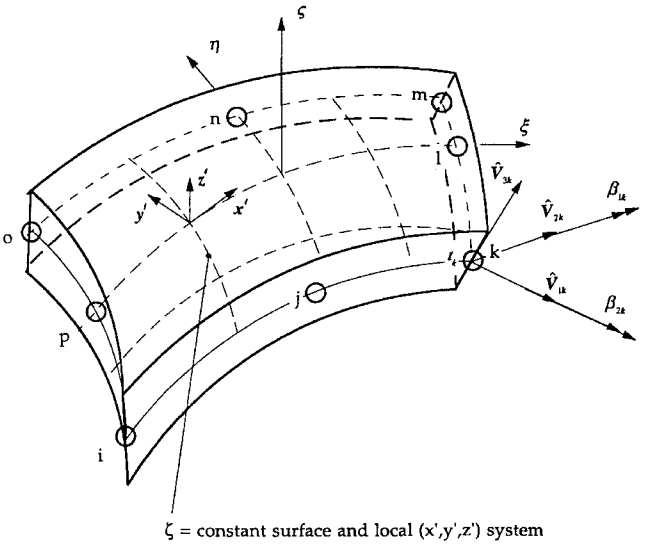

ζ = constant surface and local (x',y',z') system

Fig. 1 Coordinate systems.

The corresponding relation for the preceding U is obtained as

$$U = J^{-1}V \tag{9b}$$

where

$$V = \begin{bmatrix} u_{,\xi} & v_{,\xi} & w_{,\xi} \\ u_{,\eta} & v_{,\eta} & w_{,\eta} \\ u_{,\zeta} & v_{,\zeta} & w_{,\zeta} \end{bmatrix} \tag{9c}$$

and

$$J = \begin{bmatrix} x_{,\xi} & y_{,\xi} & z_{,\xi} \\ x_{,\eta} & y_{,\eta} & z_{,\eta} \\ x_{,\zeta} & y_{,\zeta} & z_{,\zeta} \end{bmatrix} \tag{9d}$$

Hence, a typical strain-displacement interpolation matrix is obtained as

$$\varepsilon = B\delta \tag{10}$$

where δ is the nodal unknown vector and B relates the strain components in the local coordinates to the nodal unknowns.

The corresponding stress components are obtained from

$$\sigma = D\varepsilon$$

where D is the elasticity matrix, ε is represented in Eq. (8), and

$$\sigma^T = [\sigma_{x'}, \sigma_{y'}, \tau_{x'y'}, \tau_{x'z'}, \tau_{y'z'}]$$

Having the expressions for strain-displacement and stress-strain relationships, the element stiffness matrix K^e and internal force vector f^e are also defined as follows:

$$K^e = \int_{v^e} B^T DB dV$$

$$f^e = \int_{v^e} B^T \sigma dV$$

For the elastoplastic stress-strain relationship, the total strain increment $d\varepsilon$ can be expressed as

$$d\varepsilon = d\varepsilon^e + d\varepsilon^p$$

The stress increment $d\sigma$ is determined by

$$d\sigma = D d\varepsilon^e$$

whereas the plastic strain increment is obtained by the flow rule:

$$d\varepsilon^p = \frac{d\lambda \partial \Phi}{\partial \sigma}$$

where Φ = plastic potential and dλ = proportional constant. The stress-strain relationship is given by

$$d\sigma = D_{ep} d\varepsilon$$

Hence, the tangental stiffness matrix of the elastoplastic material is given as

$$K^e = \int_{v^e} B^T D_{ep} B dV$$

The eight-noded serendipity shell element and the nine-noded Heterosis shell element have been employed in the present study.

The element(s) interpolation functions for approximating the dependent variable variation are briefly summarized next.

Shape functions:

1) Eight-node serendipity element corner nodes:

$$N_i = \tfrac{1}{4}(1 + \xi\xi_i)(1 + \eta\eta_i)(\xi\xi_i + \eta\eta_i - 1)$$

$$(i = 1, 3, 5, 7) \tag{11a}$$

Midside nodes:

$$N_i = \tfrac{1}{2}\xi_i^2(1 + \xi\xi_i)(1 - \eta^2) + \tfrac{1}{2}\eta_i^2(1 + \eta\eta_i)(1 - \xi^2)$$

$$(i = 2, 4, 6, 8) \tag{11b}$$

2) Nine-node Heterosis element corner nodes:

$$N_i = \tfrac{1}{4}(1 + \xi\xi_i)(1 + \eta\eta_i)(\xi\xi_i + \eta\eta_i - 1)$$

$$(i = 1, 3, 5, 7) \tag{12a}$$

Midside nodes:

$$N_i = \tfrac{1}{2}\xi_i^2(1 + \xi\xi_i)(1 - \eta^2) + \tfrac{1}{2}\eta_i^2(1 + \eta\eta_i)(1 - \xi^2)$$

$$(i = 2, 4, 6, 8) \tag{12b}$$

Central node:

$$N_9 = (1 - \xi^2)(1 - \eta^2) \tag{12c}$$

Explicit, Unconditionally Stable, VIP Time Integral Methodology

Following the standard assembly procedures, the governing N-DOF equations for nonlinear structural dynamics problems without damping are expressed as

$$Ma + f(d) = P(t) \tag{13}$$

where vector d and a are the displacement and acceleration fields of the system, respectively, $f(d)$ is the internal force vector, P is the applied external force vector, and t represents time. The mass matrix M for structural dynamics, in general, is positive definite and symmetric. The specified initial conditions are typically

$$d(0) = d_0 \qquad \text{and} \qquad v(0) = v_0 \tag{14}$$

The general nonlinear structural dynamics problem can also be represented as follows:

$$Ma + K_0 d = F(d) \tag{15a}$$

where the nonlinear force vector $F(d)$ is given by

$$F(d) = P(t) - f(d) + K_0 d \tag{15b}$$

and the matrix K_0 is the stiffness matrix evaluated at the initial state of the dynamic system. Physically, the nonlinear force vector $F(d)$ is equivalent to the residual force plus $K_0 d$.

For the time discretization, following our previous efforts relevant to the theoretical developments,[1,2] the basic idea involved emanates from a weighted residual approach employed for the time discretization, wherein instead of employing standard polynomial functions for the time weighting functions (which lead to various types of finite difference approximations), we seek to account for the physics of the representative dynamic behavior of the transient problem via a virtual displacement field that is uniquely selected as time weighting functions obtained from a knowledge of the eigenproblem at the initial state.

As a consequence, time discretization of the general nonlinear dynamic problem, Eqs. (15), is proposed via

$$\int_t^{t+\Delta t} W^T [Ma + K_0 d - F(d)]\, dt = 0 \tag{16}$$

where $W = W(t)$ seeks to account for the physics of the dynamic behavior via a virtual displacement field selected by imposing

$$M\ddot{W} + K_0 W = MX\delta(t - \tau) \qquad \tau \in [t, t + \Delta t] \tag{17a}$$

and X is obtained from a solution of the eigenproblem at the initial state

$$K_0 X - MX\Omega^2 = 0 \tag{17b}$$

Table 1 Explicit VIP time integral methodology

Step 1. Evaluate the finite element semidiscretized mass matrix $\boldsymbol{M}$ and initial stiffness matrix $\boldsymbol{K}$.

Step 2. Solve the linear eigenproblem $\boldsymbol{K}_0\boldsymbol{X} - \boldsymbol{M}\boldsymbol{X}\boldsymbol{\Omega}^2 = 0$ for eigenvector $\boldsymbol{\Omega}^2$ and eigenvalues $\boldsymbol{X}$.

Step 3. Determine initial conditions in generalized coordinates

$$\boldsymbol{q}(0) = \boldsymbol{X}^T\boldsymbol{M}\boldsymbol{d}(0)$$
$$\dot{\boldsymbol{q}}(0) = \boldsymbol{X}^T\boldsymbol{M}\dot{\boldsymbol{d}}(0)$$

Step 4. Enter time step loop. Compute the equivalent residual force $\boldsymbol{F}^{*k}_{n+1}$ by

$$\boldsymbol{F}^{*k}_{n+1} = \boldsymbol{P}^*_{n+1} - \boldsymbol{f}^*_{n+1} + \boldsymbol{\Omega}^2\boldsymbol{q}^*_{n+1}.$$

Step 5. Compute explicitly the current displacement and velocity field in the generalized coordinates (note that no system equations need to be solved):

$$\begin{Bmatrix} \boldsymbol{q}^{k+1}_{n+1} \\ \dot{\boldsymbol{q}}^{k+1}_{n+1} \end{Bmatrix} = \begin{bmatrix} \cos\boldsymbol{\Omega}\Delta t & \boldsymbol{\Omega}^{-1}\sin\boldsymbol{\Omega}\Delta t \\ -\boldsymbol{\Omega}\sin\boldsymbol{\Omega}\Delta t & \cos\boldsymbol{\Omega}\Delta t \end{bmatrix} \left(\begin{Bmatrix} \boldsymbol{q}_n \\ \dot{\boldsymbol{q}}_n \end{Bmatrix} + \begin{bmatrix} \boldsymbol{\alpha}_1 & \boldsymbol{\alpha}_3 \\ \boldsymbol{\alpha}_2 & \boldsymbol{\alpha}_4 \end{bmatrix} \begin{Bmatrix} \boldsymbol{F}^*_n \\ \boldsymbol{F}^{*k}_{n+1} \end{Bmatrix} \right)$$

Step 6. Check convergence of displacement and velocity fields. If converged, update

$$\boldsymbol{d}(t_{n+1}) = \boldsymbol{X}\boldsymbol{q}(t_{n+1}) = \boldsymbol{X}\boldsymbol{q}_{n+1} = \sum_{i=1}^{m} \boldsymbol{X}_i q_i(t_{n+1})$$
$$\dot{\boldsymbol{d}}(t_{n+1} = \boldsymbol{X}\dot{\boldsymbol{q}}(t_{n+1}) = \boldsymbol{X}\dot{\boldsymbol{q}}_{n+1} = \sum_{i=1}^{m} \boldsymbol{X}_i \dot{q}_i(t_{n+1})$$

and then go to step 4 for next time step; otherwise, go to step 4 for next iteration.

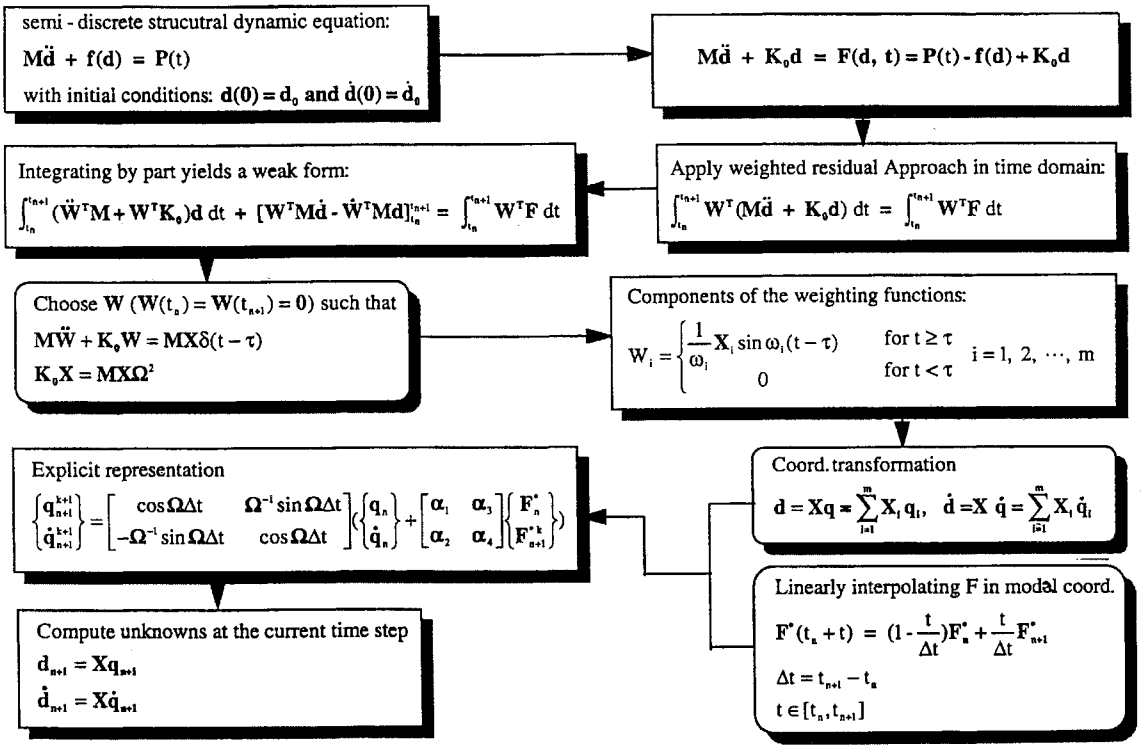

Fig. 2 Flowchart illustrating theoretical developments: VIP time integral methodology.

The preceding developments lead to an explicit, unconditionally stable, time integral methodology of computation with excellent algorithmic attributes and computationally attractive numerical solution features. The resulting time integral methodology capitalizes on the advantages of both time integration methods and mode superposition and for general nonlinear dynamics of shell structures is summarized in Table 1 (a flowchart detailing the developments is shown in Fig. 2):

In Table 1 matrices $\boldsymbol{\Omega}^2$ and $\boldsymbol{X}$ are $N \times m$, where N is the number of unknowns and m is the number of eigenpairs involved in the given computation. The vectors $\boldsymbol{q}$ and $\dot{\boldsymbol{q}}$ are the generalized displacement and velocity fields, respectively, and are only m in length. The superscript k represents the iteration and the subscript n represents the time station.

The variables $\boldsymbol{P}^*$ and $\boldsymbol{F}^*$ are given by

$$\boldsymbol{P}^* = \boldsymbol{X}^T\boldsymbol{P} \tag{18a}$$

$$\boldsymbol{F}^* = \boldsymbol{X}^T\boldsymbol{F} \tag{18b}$$

and the diagonal coefficient matrices $\boldsymbol{\alpha}_i$ $(i = 1, 2, 3, 4)$ are defined as

$$\boldsymbol{\alpha}_1 = \boldsymbol{\Omega}^{-2}[(\Delta t\boldsymbol{\Omega})^{-1}\sin\boldsymbol{\Omega}\Delta t - \boldsymbol{I}]$$

$$\boldsymbol{\alpha}_2 = \frac{\boldsymbol{\Omega}^{-2}(\boldsymbol{I} - \cos\boldsymbol{\Omega}\Delta t)}{\Delta t} \tag{18c}$$

$$\boldsymbol{\alpha}_3 = \boldsymbol{\Omega}^{-2}[\cos\boldsymbol{\Omega}\Delta t - (\Delta t\boldsymbol{\Omega})^{-1}\sin\boldsymbol{\Omega}\Delta t]$$

$$\boldsymbol{\alpha}_4 = \boldsymbol{\Omega}^{-1}[\sin\boldsymbol{\Omega}\Delta t + (\Delta t\boldsymbol{\Omega})^{-1}(\cos\boldsymbol{\Omega}\Delta t - \boldsymbol{I})]$$

and $\Delta t = t_{n+1} - t_n$ is the time increment.

We can make the following summary:

1) For general nonlinear dynamic situations, the time integral methodology of computation is explicit (the solution of system equations are not involved) with iteration. For a linear model, the solution is obtained in one iteration. The implementation of the methodology is very simple and the iteration procedure is standard. Currently

available codes for obtaining internal force can be employed for F^*_{n+1}.

2) The eigenproblem at the initial state, governed by $K_0X - MX\Omega^2 = 0$, is only solved once for merely obtaining the time weighting functions for the entire transient period.

3) In the derivation of the methodology, the general nonlinear tangent matrix K for the dynamic system is actually accounted for and employed, and thus the explicit methodology developed is suitable for general nonlinear computational structural dynamic situations.

4) Since no finite difference approximations are involved in the formulations, the approach yields a unique solution methodology that is explicit and is also directly self-starting and eliminates the need to involve accelerations in the computations.

5) The explicit nature of the methodology necessitates only vector operations. In addition, the dimensions of matrices and vectors involved are only m instead of N; usually m is significantly less than N (m is the number of modes employed and N is total system DOF).

Illustrative Applications

Illustrative numerical examples are described next with emphasis on applications to realistic engineering problems of practical interest.

Example 1. Dynamic Response of an Elastoplastic Clamped Arch

An elastoplastic arch clamped at both ends and subjected to a uniform constant pressure on the top surface is studied. The geometry and material properties of the arch are shown in Fig. 3. The finite element mesh and element information are also given in Fig. 3. Because of the symmetric geometry and loading condition, half of the arch is analyzed with 10 nine-node, four-layer Heterosis shell elements. In the analysis, there are a total of 208 unknowns to be determined. The dynamic responses of both the elastic and elastoplastic arch are plotted in Figs. 4 and 5, respectively. The comparative CPU times on the Cray 2 supercomputer for the VIP method and Newmark implicit and explicit methods are listed in Tables 2 and 3, respectively.

For the elastic arch, both the VIP method with 25 modes and the Newmark implicit as well as the explicit method have comparable accuracy. However, while the VIP method has significant CPU advantage over the explicit method, comparing with the implicit method for a short transient period, the implicit method took less computing time, but for a longer transient period, the VIP method demonstrated an improved CPU advantage. For this case, when t_{end} is about 0.05 s, the VIP method begins to show the CPU advantage. The reason that the VIP method took more CPU time than the implicit method for a shorter transient period is that it takes about 3 s to compute 25 eigenpairs. A smaller number of modes also yields comparable accuracy of results.

For the elastoplastic arch, the Newmark implicit method is employed in conjunction with a quasi-Newton–Raphson nonlinear iterative procedure. To obtain a converged solution, the sizes of time

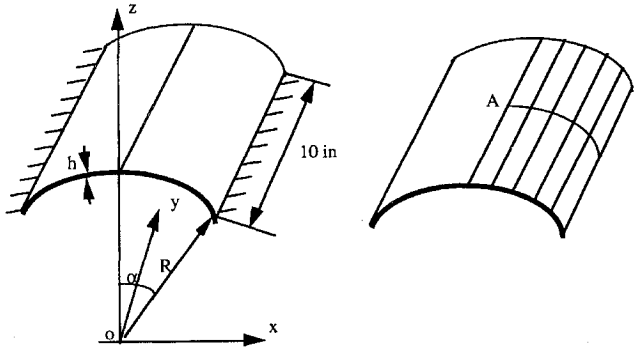

Fig. 3 Geometry, material properties, and finite element mesh for the clamped arch: R = 22.27 in., h = 0.41 in., α = 53.34 deg; material properties: $E = 10.5 \times 10^6$ psi, $E_p = 0.21 \times 10^6$ psi, p = 300 psi (on the top of the surface and constant with time), ν = 0.3, $\rho = 2.45 \times 10^{-4}$ lb-s^2/in.^{4}, σ_y = 24,000 psi; and total number of elements = 10 (nine-node heterosis element), total number of nodes = 55; total number of layers = four, and total number of DOF = 208.

Table 2 CPU time on Cray 2 for the dynamic analysis of the elastic arch

Methods	Δt, s	t_{end}, s	n steps	CPU time, s	Speed-up
Newmark explicit	5.0e−7	0.01	20,000	35.8	10
Newmark implicit	5.0e−5	0.01	200	1.7	0.47
VIP: 25 mode	5.0e−5	0.01	200	3.6	——
Newmark explicit	5.0e−7	0.05	100,000	172.3	44
Newmark implicit	5.0e−5	0.05	1,000	4.5	1.15
VIP: 25 mode	5.0e−5	0.05	1,000	3.9	——

Table 3 Comparative CPU time on Cray 2 for the dynamic analysis of the elastoplastic arch

Methods	Δt, s	t_{end}, s	n steps	CPU time, s	Speed-up
Newmark explicit	5.0e−7	0.01	20,000	1378	25.5
Newmark implicit	5.0e−6	0.01	2,000	286	5.3
Newmark implicit	5.0e−5	0.01	200	N/A	——
VIP: 65 mode	5.0e−5	0.01	200	54	——

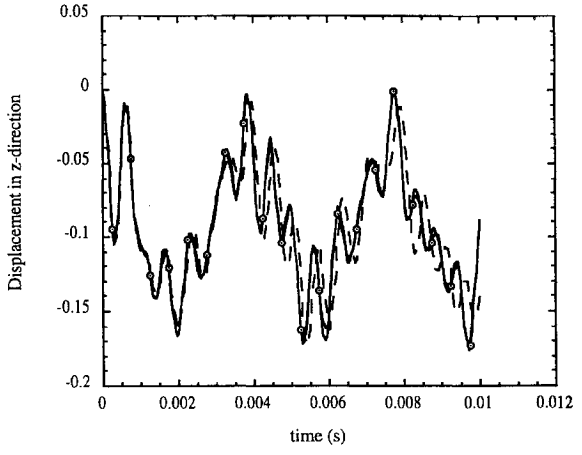

Fig. 4 Dynamic response of the elastic arch structure: —·—, VIP: 25-mode, Δt = 5.0e−5; - - - -, Newmark implicit: Δt = 5.0e−5; and ——, Newmark explicit: Δt = 5.0e−7.

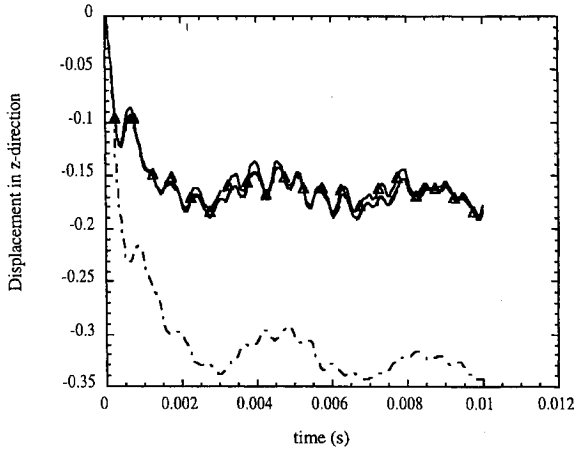

Fig. 5 Dynamic response of the elastoplastic arch: ——, Newmark explicit: Δt = 5.0e−7; - - - -, Newmark implicit: Δt = 5.0e−6; ·····, Newmark implicit: Δt = 5.0e−5; and —△—, VIP: 65-mode, Δt = 5.0e−5.

steps taken were 5.0×10^{-7}, 5.0×10^{-6}, and 5.0×10^{-5} for the Newmark explicit, implicit, and VIP methods, respectively. From the dynamic response shown in Fig. 5, when $\Delta t = 5.0 \times 10^{-5}$ was taken for the Newmark implicit method, the accuracy of the solution is poor; however, the VIP method provided an accurate solution. This implies that the VIP method has improved stability characteristics over the Newmark implicit ($\beta = 0.25$ and $\gamma = 0.5$) method. On the other hand, the VIP method has tremendous CPU advantage over both the explicit and implicit Newmark methods. The speed-up factor is up to 25.5 and 5.3 over the explicit and implicit

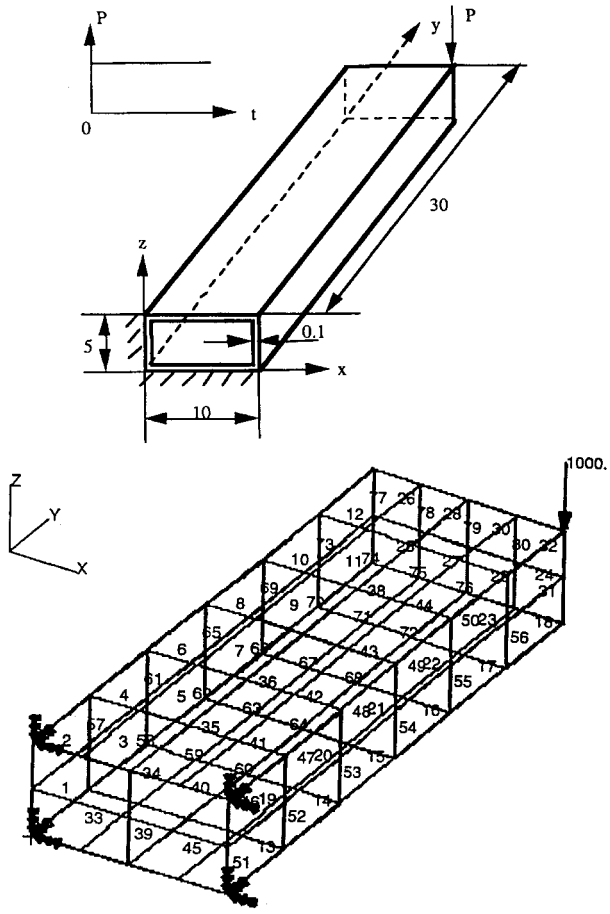

Fig. 6 Geometry, material properties, and finite element mesh for the box structure: $E = 10.5 \times 10^6$ psi, $E_p = 0.21 \times 10^6$ psi, $P = 400$ lb (for the elastic case); $\nu = 0.3$, $\rho = 2.45 \times 10^{-4}$ lb-s^2/in.^{4}, $P = 1000$ lb (for the elastoplastic case); and $\sigma_y = 24000$ psi, total nodes = 253, total elements = 80, total DOF = 1145; element type: eight-node, four-layer serendipity shell.

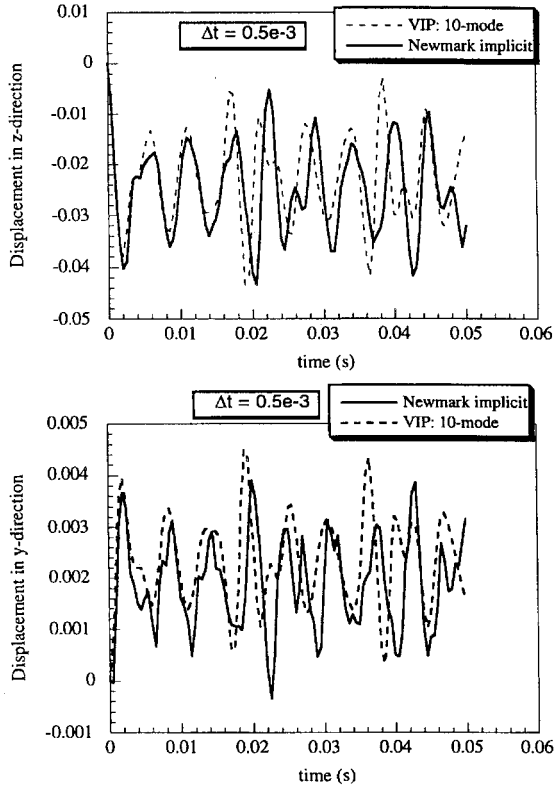

Fig. 7 Dynamic responses of the elastic box structure at the loading point.

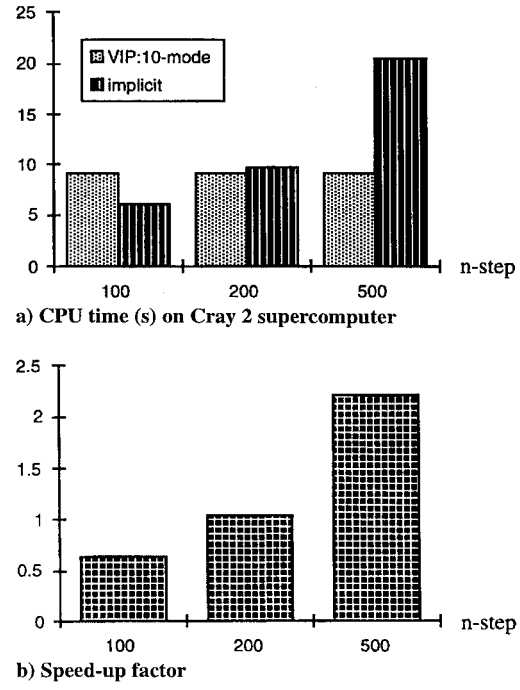

Fig. 8 Comparative CPU time and speed-up factor for the elastic box structure.

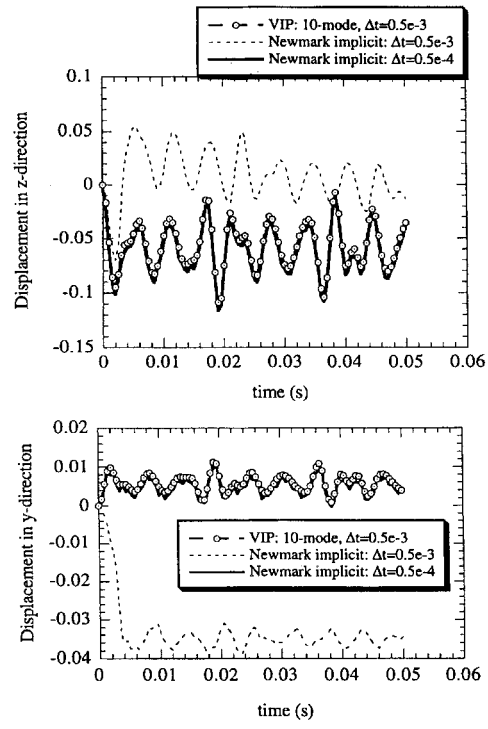

Fig. 9 Dynamic responses of the elastoplastic box structure at the loading point.

methods with a quasi-Newton–Raphson procedure, even for a short transient period of 0.01 s. A much higher speed-up factor can be expected for longer transient periods.

Example 2. Dynamic Response of an Elastoplastic Box Structure

The next example is a cantilever box structure subjected to a concentrated load P. The geometry, material properties, loading conditions, and finite element mesh of the structure are given in Fig. 6. The dynamic responses of the elastic structure and the comparative CPU and speed-up obtained from the VIP method and the Newmark implicit method are plotted in Figs. 7 and 8, respectively. The comparative results for the elastoplastic case of the VIP method and the implicit method (trapezoidal rule) are shown in Figs. 9 and 10

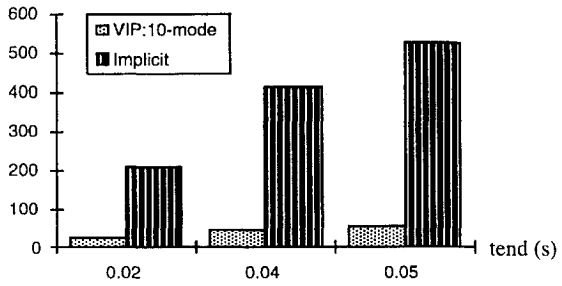

a) CPU time (s) on Cray 2 supercomputer

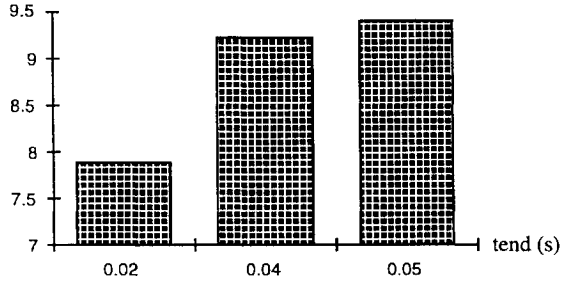

b) Speed-up factor

Fig. 10 Comparative CPU time and speed-up factor for the elastoplastic box structure.

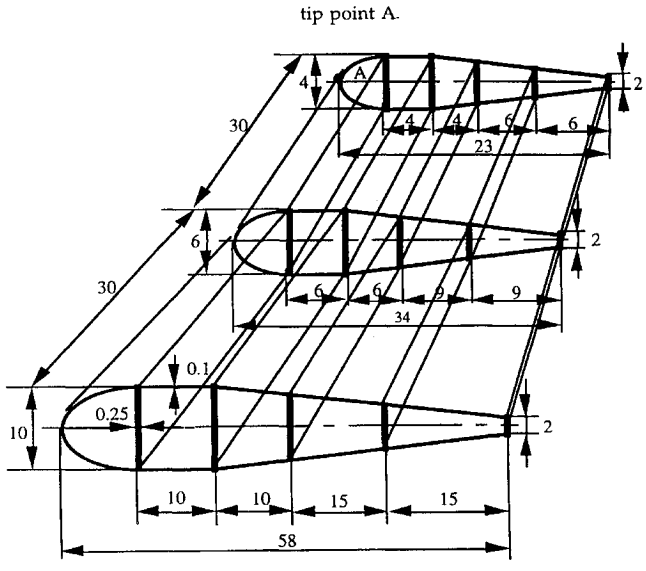

Fig. 11 Geometry and material properties of the wing structure: E = 10.5 × 10^6 psi, E_p = 0.21 × 10^6 psi, P = 20 psi (on the top of surface and constant with time); ν = 0.3, ρ = 2.45 × 10^{-4} lb-s^2/in.^{4}; and σ_y = 24,000 psi.

for the respective cases (a quasi-Newton–Raphson is used for the nonlinear case with the implicit Newmark method).

In the dynamic analysis of the elastic box, the comparative CPU time and speed-up factor are reported in terms of number of time steps involved, because both the Newmark implicit and the VIP method are unconditionally stable, and the computational performance for these two methods is strictly related to the number of the time steps if the same Δt is used. For the VIP method, most of the computing time was spent on calculating the eigenproblem; solving the time integral only takes a fraction of the time for the eigenproblem. This is clearly demonstrated in Fig. 8. From Fig. 8, the VIP method almost took the same amount of CPU time for 100, 200, and 500 time steps. This is not only because of the high speed of the Cray 2 computer but also because the eigenproblem takes most of the computing time. However, for the Newmark implicit method (trapezoidal rule), the CPU time increases with more time steps involved. After about 200 time steps, the VIP method demonstrates the CPU time advantage, and the advantage increases with more time steps involved.

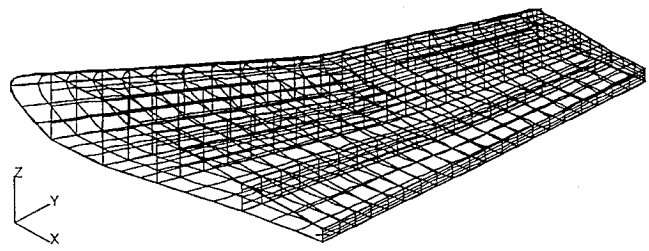

Fig. 12 Finite element mesh for the wing structure: total number of nodes = 3043, total number of elements = 1056 (eight-node serendipity shell element with four layers), and total number of DOF = 14,735.

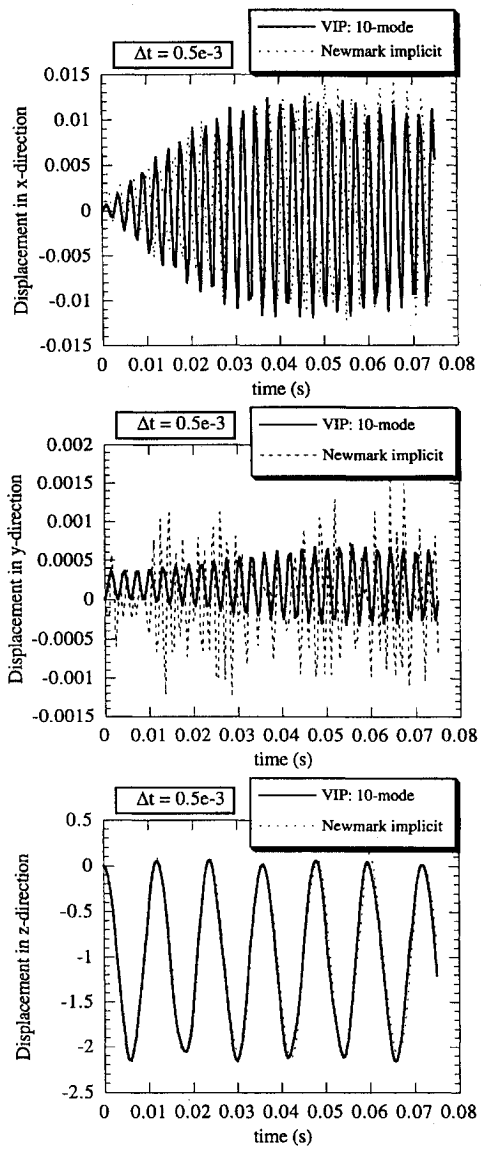

Fig. 13 Dynamic responses of the elastic wing structure at the tip point A.

For the elastoplastic box structure, the VIP method has a tremendous CPU time advantage even for the transient period time of 0.05 s in comparison with the Newmark implicit method with a quasi-Newton–Raphson scheme. The speed-up factor reaches 9.4. When $\Delta t = 0.5 \times 10^{-3}$ was adopted in the analysis, the Newmark implicit method (trapezoidal rule) converged to an inaccurate answer, whereas the VIP method provided an excellent result. On the other hand, the VIP method took only 56 s whereas the trapezoidal rule took about 70 s of CPU time on the Cray 2 supercomputer. For this structure, the trapezoidal rule needed a $\Delta t = 0.5 \times 10^{-4}$ to obtain an accurate solution. In Fig. 10, the comparative CPU time of the implicit method reported was based on $\Delta t = 0.5 \times 10^{-4}$. The computing times of three different transient periods, namely, 0.02,

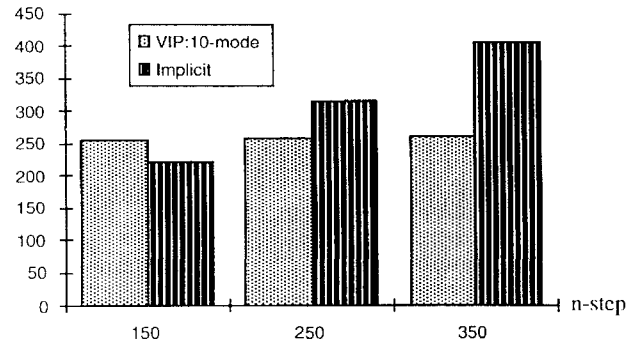

a) CPU time (s) on Cray 2 supercomputer

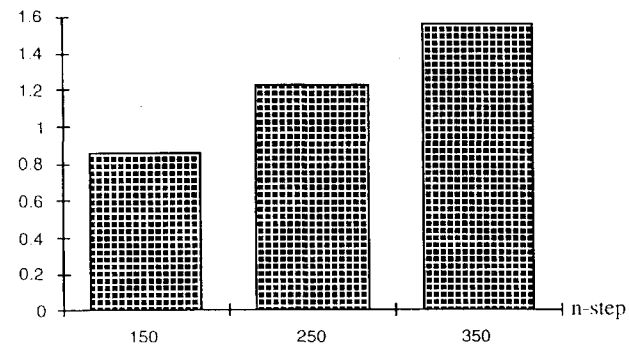

b) Speed-up factor

Fig. 14 Comparative CPU time and speed-up factor for the elastic wing structure.

0.04, and 0.05 s, are reported in Fig. 10. The VIP method with 10 modes took between 27 and 56 s, whereas the trapezoidal rule took between 210 and 528 s. Obviously, the speed-up factor of the VIP method vs the trapezoidal rule ranges from 7.8 to 9.4. This example also clearly shows that the VIP method has improved stability characteristics over the Newmark implicit (trapezoidal rule) method for the linear and nonlinear cases.

Example 3. Dynamic Response of an Elastic Wing Structure

The dynamic response of a large-scale wing structure is investigated in this section. The geometry and material properties of the wing are given in Fig. 11. The finite element mesh is shown in Fig. 12. Inside of the wing, there are four vertical panels to support the skin of the wing, and the larger end of the wing is clamped. For the mesh, there are a total of 3043 nodes, 1056 eight-node serendipity shell elements, and 14,735 DOF. In the analysis, each eight-node shell element was divided into four layers. The wing structure is subjected to a uniform pressure of 20 psi on the top of the surface with consideration of gravity effects. The applied pressure is assumed constant with time.

An elastic dynamic analysis of the wing is first considered here for illustration employing the VIP method and the Newmark implicit method. The dynamic responses at the tip point A for the elastic wing are shown in Fig. 13. The comparative computing times on the Cray 2 supercomputer are reported in Fig. 14.

For the dynamic response of the elastic wing, both methods agree with each other well, except for the displacement history in the y direction where the VIP method with 10 modes damped out the high-frequency effects, thereby smoothing out the numerical response. For the VIP method, the size of the time step can also be taken to be much larger than that used for the analysis to show the smooth curve for the displacement history ($\Delta t = 0.5E - 3$ is used here). When a larger Δt is taken, the same response accuracy is obtained by using the VIP method. The comparative CPU times and speed-up factors are shown in Fig. 14. Similar to the dynamic analysis of the box structure, the speed-up factor increases with the number of time steps. In this case, after about 250 steps, the VIP method shows an improved CPU time advantage. The example clearly showed the applicability to a realistic large-scale dynamic built-up shell wing structure.

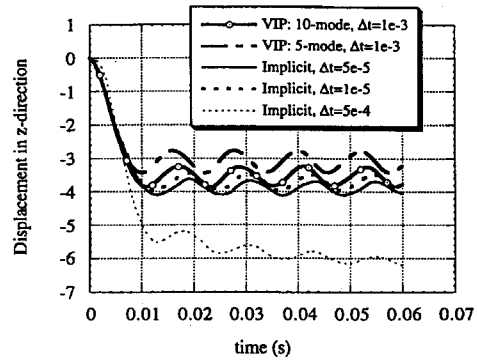

a) Comparative dynamic responses in z direction obtained by the VIP method and the Newmark implicit method

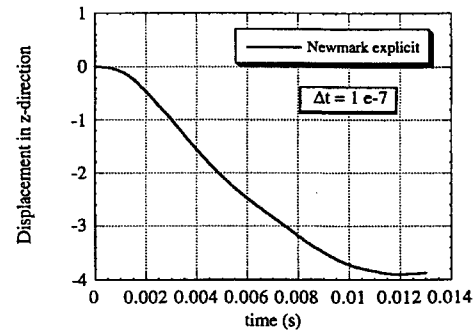

b) Dynamic response in z direction obtained by the Newmark explicit method

Fig. 15 Dynamic responses of the elastoplastic wing structure of tip point A.

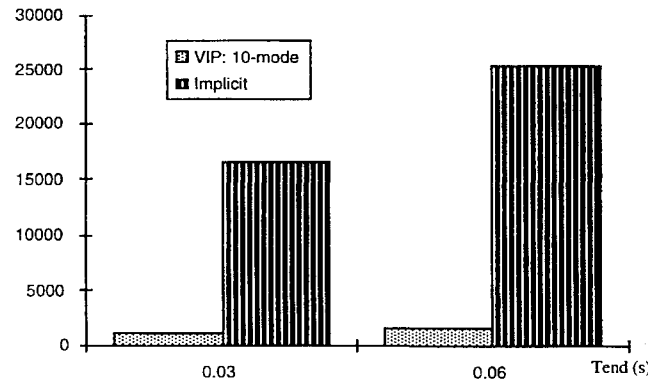

a) CPU time (s) on Cray 2 supercomputer

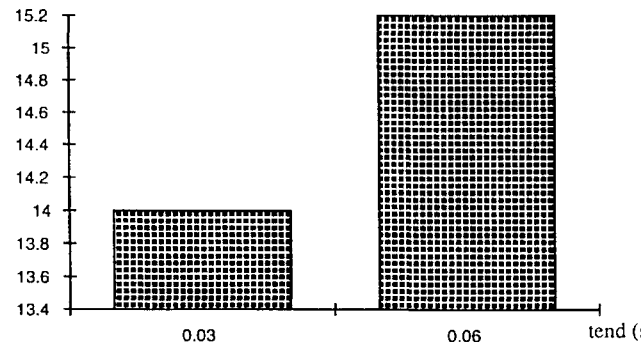

b) Speed-up factor on Cray 2 supercomputer

Fig. 16 Comparative CPU time and speed-up factor for elastoplastic wing structure.

For the elastoplastic wing structure, the comparative displacement histories in the downward z direction are shown in Fig. 15a. For the purpose of fairness and comparison with the VIP results, we have selected $\Delta t = 5.0 \times 10^{-5}$ as an acceptable solution via the Newmark method (although $\Delta t = 1.0 \times 10^{-5}$ is a more accurate solution). The accuracy is also validated with the explicit Newmark method (Fig. 15b) $\Delta t = 1.0 \times 10^{-7}$ for a total duration of 0.013 s,

for which the CPU was 391,785 s (this analysis was conducted primarily to have an accurate estimate of the peak value). As evident, with only 10 modes involved and a fairly large $\Delta t = 1.0 \times 10^{-3}$, the VIP gives a converged solution and its accuracy is comparable. For given accuracy conditions, the comparative implicit Newmark ($\Delta t = 5.0 \times 10^{-5}$) and the explicit VIP ($\Delta t = 1.0 \times 10^{-3}$) CPU times and the speed-up factors are shown in Fig. 16 for $t_{\text{end}} = 0.03$ and 0.06 s, respectively. It should be noted that the longer the transient (period) analysis, the higher the speed-up factor results.

Concluding Remarks

A generalized computational methodology for the dynamic analysis of elasticplastic/elastic shell structures in conjunction with an explicit VIP methodology has been described with details outlining the computational implementation issues and numerical aspects. The stability and accuracy characteristics and computational attributes of the explicit, unconditionally stable, second-order VIP method were briefly highlighted for illustration. The applicability and evaluation of the VIP method to practical shell structural configurations, which employed degenerated shell elements, were discussed through various numerical examples. The numerical results showed that the VIP method is effective and efficient for nonlinear structural dynamics problems and has improved accuracy and significant CPU advantage in comparison with the most commonly used Newmark family of methods. Also, the methodology is a viable alternative to traditional practices with the numerical and computational features well suited for large-scale problems and also applicable to high-speed computing environments.

Acknowledgments

The authors are very pleased to acknowledge the support of this research, in part, by NASA Johnson Space Center/LESC, Houston, TX. Partial support by the U.S. Army High Performance Computing Research Center at the University of Minnesota, on a contract from the U.S. Army Research Office, and the MSI, Minneapolis, MN, are gratefully acknowledged. Special thanks are due to more recent support of related activities by William Mermagen Sr. and Andrew Mark of the U.S. Army Research Laboratory, Aberdeen, MD.

References

[1]Sha, D., Chen, X., and Tamma, K. K., "Virtual-Pulse Time Integral Methodology: A New Computational Approach for Computational Dynamics, Part 1: Theory for Linear Structural Dynamics," *Proceedings. New Methods in Transient Analysis* (Anaheim, CA), PVP-VOL. 246/AMD-Vol. 143, American Society of Mechanical Engineers, New York, 1992.

[2]Chen, X., Tamma, K. K., and Sha, D., "Virtual-Pulse Time Integral Methodology: A New Explicit Approach for Computational Dynamics—Theoretical Developments for General Nonlinear Structural Dynamics," *Proceedings of the AIAA 34th Structural Dynamics Conference*, AIAA, Washington, DC, 1993 (AIAA Paper 93-1330).

[3]Zienkiewicz, O. C., *The Finite Element Method*, 3rd ed., McGraw–Hill, New York, 1977.

[4]Ahmad, S., Irons, B. M., and Ziekiewicz, O. C., "Analysis of Thick and Thin Shell Structures by Curved Finite Elements," *International Journal for Numerical Methods in Engineering*, Vol. 2, 1970, pp. 419–451.

[5]Owen, D. R. J., and Hinton, E., *Finite Element in Plasticity: Theory and Practice*, Pineridge, Swansea, Wales, UK, 1980.

[6]Hinton, E., and Owen, D. R. J., *Finite Element Software for Plates and Shells*, Pineridge, Swansea, Wales, UK, 1984.

[7]Owen, D. R. J., and Li, Z. H., "Elastic-Plastic Dynamic Analysis of Anisotropic Laminated Plates," *Computer Methods in Applied Mechanics and Engineering*, Vol. 70, 1988, pp. 349–365.

[8]Bathe, K. J., *Finite Element Procedures in Engineering Analysis*, Prentice–Hall, Englewood Cliffs, NJ, 1982.

[9]Wilson, E. L., Farhoomand, I., and Bathe, K. J., "Nonlinear Dynamic Analysis of Complex Structures," *Earthquake Engineering and Structural Dynamics*, Vol. 1, 1973, pp. 241–252.

[10]Newmark, N. M., "A Method of Computation for Structural Dynamics," American Society of Civil Engineers, ASCE-EMS, New York, 1959, pp. 67–94.

[11]Hughes, T. J. R., *The Finite Element Method*, Prentice–Hall, Englewood Cliffs, NJ, 1987.

[12]Tamma, K. K., Chen, X., and Sha, D., "Recent Advances Towards a Virtual-Pulse (VIP) Time Integral Methodology for General Structural Dynamics Problems: Theoretical Developments and Implementation Aspects," *Proceedings of the 1993 ASME Winter Annual Meeting* (New Orleans, LA), American Society of Mechanical Engineers, New York, 1993.